Density Functional Theory Investigation of Cobalt Siting in Ferrierite

Scott A. McMillan, Linda J. Broadbelt,* and Randall Q. Snurr*

Institute for Environmental Catalysis and Department of Chemical Engineering, 2145 Sheridan Road, Northwestern University, Evanston, Illinois 60208-3120

Received: January 23, 2002; In Final Form: June 19, 2002

Cobalt-exchanged ferrierite is a selective catalyst for the reduction of nitrogen oxides in the presence of oxygen. The activity of each isolated cobalt cation has been suggested to depend on the local zeolite environment. Two of the three cobalt extraframework sites proposed in the literature were investigated with density functional theory calculations. The electronic structure, geometry, and infrared spectra of eight clusters were calculated and compared to experiment. Exchanged cobalt cations were most stable in the high-spin electronic configuration. The stability of cobalt in each site was evaluated by calculating the cobalt−zeolite binding energy. The calculations also show the important role of zeolite aluminum location in extraframework cobalt siting. Only one of the eight clusters was able to reproduce all of the experimental characteristics of the predominant cobalt species. A secondary cobalt species was predicted to most likely correspond to one of four possible candidate clusters.

Introduction

In light of limited petroleum reserves and stricter air pollution standards, lean burn engines for vehicles are increasingly attractive since they are more fuel efficient than normal gasoline engines and consequently emit less carbon dioxide. Lean burn engines, such as the diesel engine, operate at higher air/fuel ratios than gasoline engines. Nitrogen oxides (NO_x), atmospheric pollutants that cause acid rain, are not removed from lean burn exhaust by the popular three way catalyst due to the presence of oxygen. For these oxygen-rich environments, a selective catalyst is needed that preferentially reduces NO_x rather than combusting hydrocarbons with the oxygen. Previous research has shown that zeolite-based materials exchanged with transition metals selectively catalyze the reduction of NO_x with hydrocarbon reducing agents in the presence of excess oxygen.[1] Cobalt-exchanged zeolites are particularly notable for their high selective catalytic reduction (SCR) activity with methane;[2] nearly all other metal-exchanged zeolites have negligible activity with methane and require higher hydrocarbon reductants.[3] However, further research is necessary to develop commercially viable lean burn NO_x reduction catalysts.

The nature of the exchanged cobalt species and the activity of the catalyst depend on the exchange conditions.[4,5] Materials prepared by wet ion exchange contain only isolated cobalt ions. Isolated cobalt ions are exchanged in the high-spin (HS), divalent oxidation state.[6,7] Under these preparation conditions, cobalt is most active when exchanged in zeolites MFI and ferrierite (FER).[3,8] Li and Armor[8] observed that the turnover frequency of NO conversion to N_2 per cobalt ion in FER increases with increasing cobalt loading. Differences in cobalt activity as a function of the local zeolite environment and synergistic cooperation between nearby cobalt ions have been proposed as explanations for the increase in the turnover frequency with increasing cobalt loading.[9]

Wichterlová and co-workers have proposed extraframework sites for cobalt in mordenite, FER, and MFI based on diffuse reflectance ultraviolet/visible spectroscopy.[9,11,12] Extraframework sites were first proposed for mordenite by studying the differences in the ultraviolet/visible spectra with and without the presence of cocations such as cesium with known extraframework locations. In this manner, an ultraviolet/visible spectral signature was assigned to cobalt in a particular extraframework site. Similar cobalt spectral signatures were observed for FER and MFI; hence, similar zeolite extraframework locations were proposed for those zeolites.

The characterization of cobalt-exchanged FER has been expanded to include infrared spectroscopy and extended X-ray absorption fine structure (EXAFS). Both the infrared and the ultraviolet/visible spectra could be decomposed into three signatures, labeled α, β, and γ. The signatures have been proposed to correspond one-to-one with FER extraframework sites B, G, and C, respectively,[9,13] using the notation of Mortier.[14] The B site is located at the intersection of the eight- and 10-ring channels, and the G site is a six-membered ring separating two eight-ring channels (Figure 1). The C site is a boat-shaped site; cobalt exhibiting the γ signature does not adsorb NO,[13] indicating that cobalt in the C site does not participate in NO_x reduction.

The properties of metal cations exchanged in zeolites have been successfully investigated with quantum chemical calculations by several researchers.[15−22] For example, the stability of several transition metals in individual MFI extraframework sites has been probed with density functional theory (DFT),[18] and the structure of copper-exchanged FER was studied with periodic DFT calculations for single aluminum substitutions near the exchange site.[20] Rice et al.[17] calculated the interaction of small clusters representing MFI, again containing a single aluminum substitution, with cobalt hydroxide and adsorbed water. Šponer et al.[22] attempted to correlate geometrical and electrostatic cluster properties to the β FER infrared spectrum. The ultraviolet/visible spectrum of cobalt-exchanged zeolite A

* To whom correspondence should be addressed. L.J.B.: broadbelt@northwestern.edu. R.Q.S.: snurr@northwestern.edu.

10.1021/jp020215q CCC: $22.00
Published on Web 10/01/2002

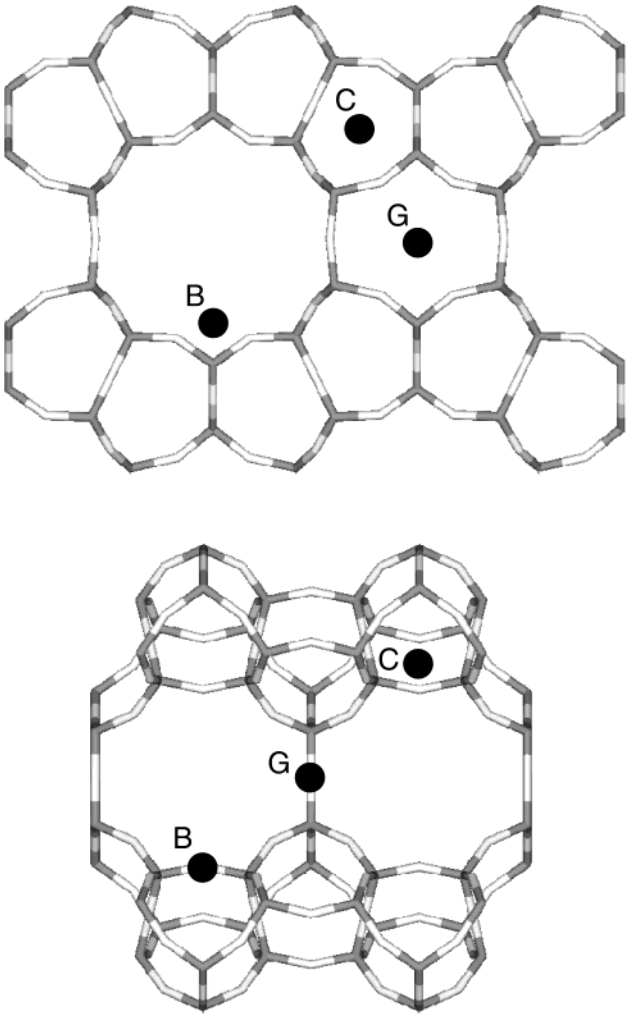

Figure 1. Location of extraframework sites B, C, and G in FER (a) looking down the 10-ring channels and (b) looking down the 8-ring channels.

has been interpreted with highly accurate ab initio calculations.[16] Very recently, the EPR signature of divalent copper-exchanged zeolites was shown to depend on the relative location of the nearby framework aluminum atoms.[23,24] The success of these and other first principles calculations of metal-exchanged zeolites supports the continued application of theoretical methods to complement and guide experimental investigations.[25]

In the present study, DFT calculations have been performed to directly compare the structure and spectral features of cobalt exchanged in different FER extraframework sites. Because the three proposed cobalt sites were not directly observed for FER but instead were based on similarities between mordenite and FER, our DFT calculations sought to confirm the assigned sites. These calculations also provide additional insight into the arrangement of aluminum centers in the cobalt ion exchange sites that cannot be determined easily from experiment.

Theoretical Methods

Before studying the stability of cobalt in different extraframework sites, the placement of the charge-compensating aluminum atoms must first be determined. Two framework aluminum atom substitutions per divalent cobalt cation are required for overall charge neutrality. The only limitation on the location of the aluminum substitutions is that aluminum centers may not share a bridging oxygen.[26] One of the T3 atoms in the site B six-membered ring and one of the T1 atoms in the site G six-membered ring[27] were arbitrarily chosen as atom 1 for numbering the T (tetrahedral) atoms of the rings. The position of the second aluminum atom can then be expressed relative to the choice of atom 1 by moving around the ring. For each site, four such symmetrically distinct arrangements are possible, denoted (1,3), (1,4), (2,5), and (2,6). The stability of divalent metal cations in zeolite extraframework sites has been suggested to be related to the distance between aluminum centers.[28−30] The distances between the T atoms in the FER X-ray diffraction (XRD) structure increase as (1,4) < (1,3) < (2,5) < (2,6) for the B site and (1,3) < (2,6) < (1,4) < (2,5) for the G site.[27]

Because the C site does not participate in NO_x reduction, the stability of cobalt in the B and G sites was the focus of the investigation. Zeolite clusters were extracted from the FER framework corresponding to sites B and G as shown in Figures 2−5. The atoms at the edge of each cluster were terminated by hydrogen atoms directed along the bond vector of what would have been the next zeolite framework atom. The Si−H and O−H distances were fixed at 1.49 and 0.98 Å, respectively. The Cartesian positions of the terminating OH and SiH_3 groups were constrained while the rest of the cluster was allowed to relax fully. The cluster size was selected to retain enough flexibility to describe any cation-induced framework distortion while minimizing the computational cost. The B-1,3, B-1,4, B-2,5, and B-2,6 clusters contain 31, 30, 32, and 32 nonhydrogen atoms, respectively, while all of the G clusters contain 29 heavy atoms.

Quantum chemical calculations utilizing the DFT formalism were applied to investigate the cobalt−zeolite interaction. The gradient-corrected functionals of Becke[31] and Perdew[32] (BP86) were used with the LANL2DZ basis set to determine the minimum energy cluster geometries using the Gaussian 98 software package.[33] The LANL2DZ effective core potential (ECP) basis set contains a double-ζ quality description of valance electrons but replaces core electrons with a potential field for a considerable computational savings. The reliability of the ECP basis was confirmed by comparing the B-1,4 ECP results to those calculated using the 6-31G* all-electron basis set.

Both a high-spin (HS) and a low-spin (LS) state of cobalt, a d^7 atom, were investigated. The HS state has three unpaired d electrons (a quartet), while the LS state has a single unpaired d electron (a doublet). Higher spin states were not considered since the electronic energy of the B-1,4 cluster in the sextet state (five unpaired electrons) was much less favorable than the quartet and doublet states. While cobalt has been shown to be exchanged only as a HS ion, the LS state may be an intermediate state in the overall NO_x reduction mechanism.[7] Ligand field theory predicts that a relatively strong ligand field produces LS ions, while a relatively weak ligand field corresponds to HS ions.

The relatively close spacing of d orbital energy levels can lead to spurious excited state configurations rather than the true ground state. The default self-consistent field (SCF) algorithm in many quantum chemical software packages only computes the first derivative of the electronic energy with respect to the orbital coefficients.[34] This scheme guarantees that the self-consistent wave function will correspond to an extreme point in orbital coefficient space but cannot distinguish between maxima, minima, and saddle points. The second derivatives must be calculated to confirm that the wave function is stable, i.e., the SCF energy corresponds to a minimum.[35]

The *stable* keyword in Gaussian 98 was employed to determine wave function stability and to correct those found to

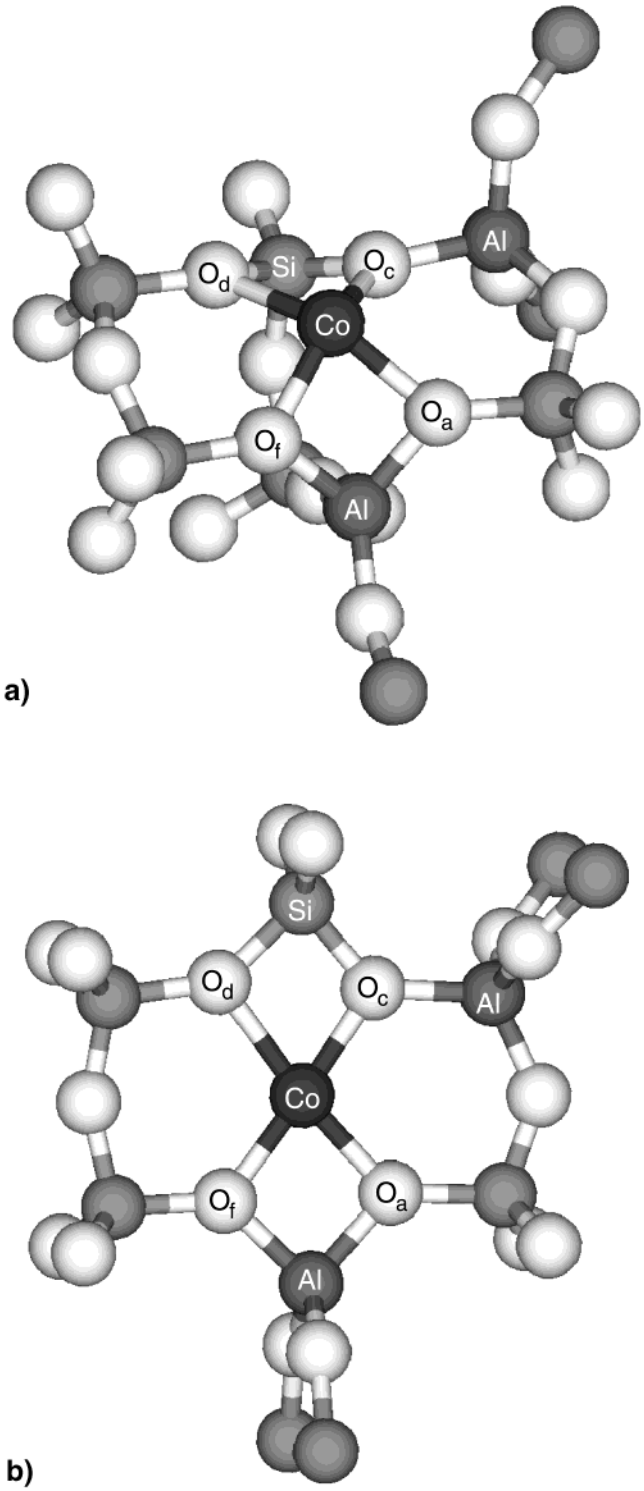

Figure 2. Structures of cobalt (a) B-1,3 and (b) G-1,3 clusters (terminating hydrogen atoms not shown).

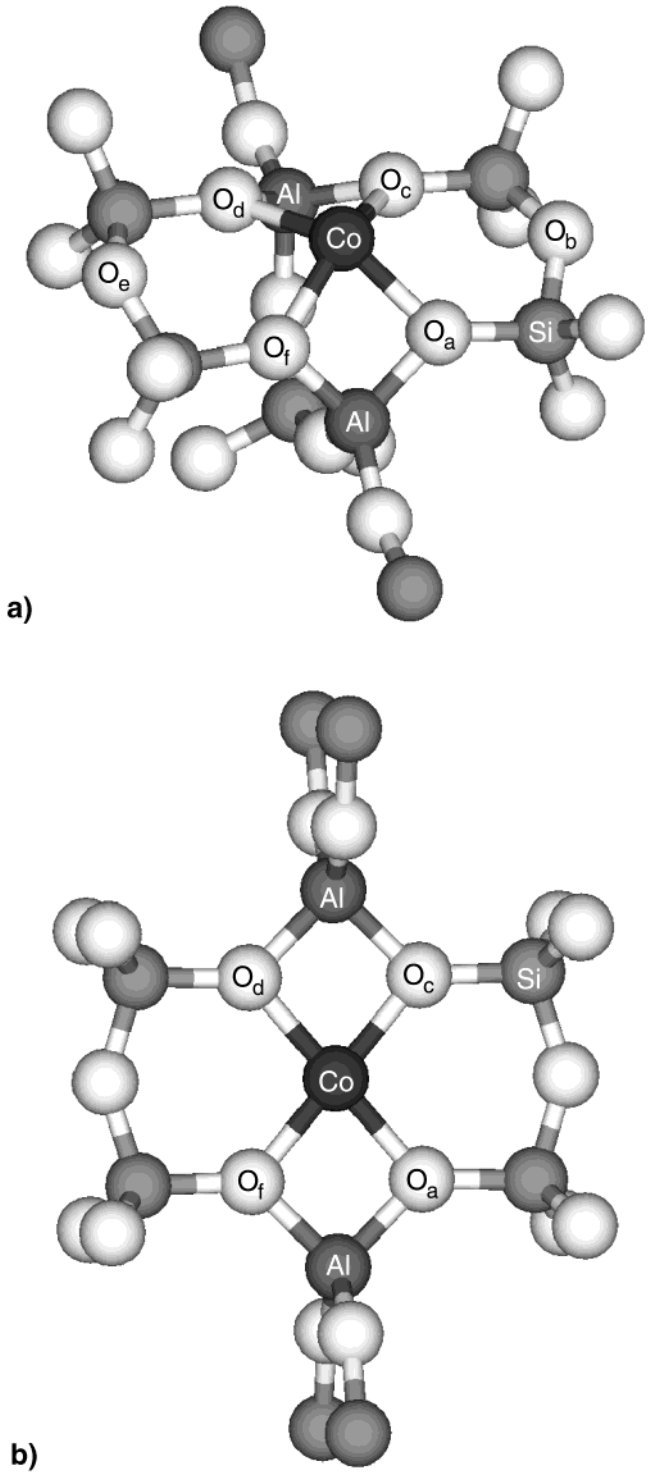

Figure 3. Structures of cobalt (a) B-1,4 and (b) G-1,4 clusters (terminating hydrogen atoms not shown).

be unstable. In the course of this investigation, two classes of wave function instabilities were encountered. The first was clearly evident from the existence of unoccupied orbitals of lower energy than occupied orbitals of the same spin. The second class, however, did not exhibit any apparent behavior to indicate the instability. The electronic energy of the unstable and stable wave function differed by hundreds of kJ/mol for the first type of instability and tens of kJ/mol for the second. The procedure used in this investigation alternated between geometry optimization and wave function stability calculations until both were satisfied.

Results

Cobalt Spin State. For both spin states, the Mulliken[36] cobalt spin density (Table 1) indicates that the unpaired electrons are localized on cobalt. The HS cobalt spin density is slightly less than 3; the remaining spin density is almost completely localized on the four framework oxygen atoms nearest to cobalt. The LS cobalt spin density agrees very well with the expected value of 1. The calculated cobalt charge is less than the formal charge, +2, indicating that the cobalt−zeolite bonding has significant covalent character.

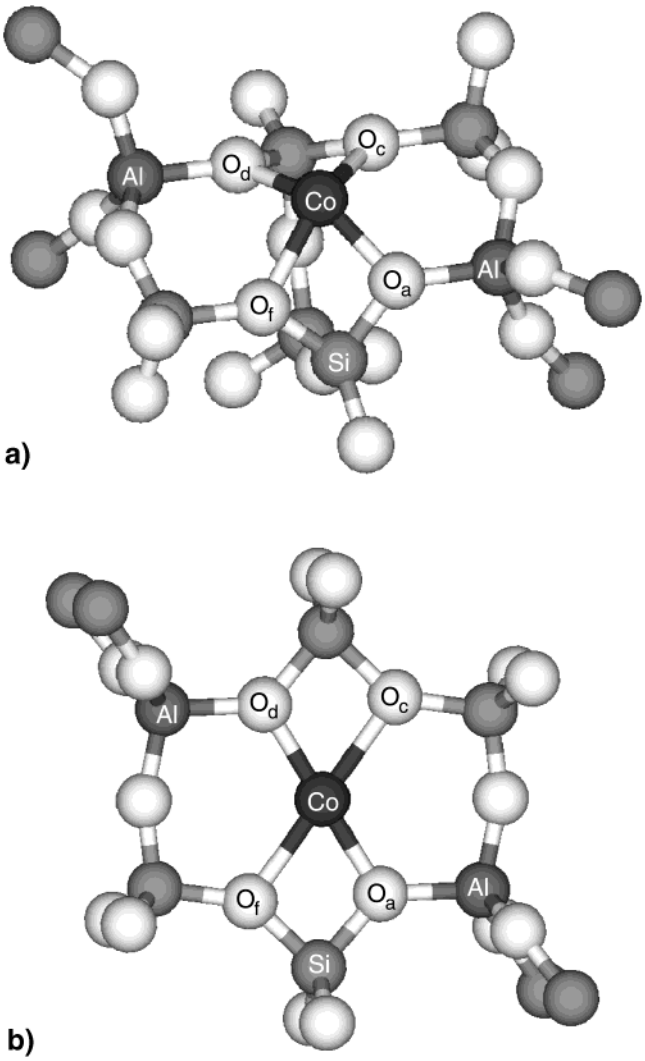

Figure 4. Structures of cobalt (a) B-2,5 and (b) G-2,5 clusters (terminating hydrogen atoms not shown).

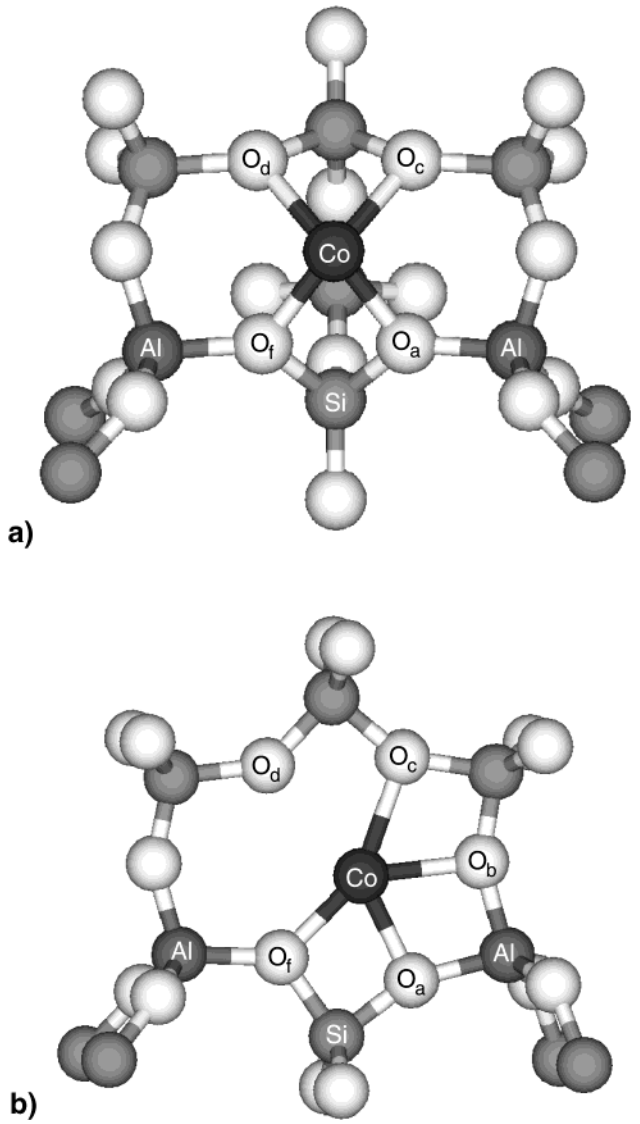

Figure 5. Structures of cobalt (a) B-2,6 and (b) G-2,6 clusters (terminating hydrogen atoms not shown).

The preferred spin state of exchanged cobalt will correspond to the state with the lowest energy. The spin energy, E_{spin}, is defined as

$$E_{spin} = E(\mathrm{HS}) - E(\mathrm{LS}) \quad (1)$$

where E(HS) is the electronic energy of the optimized HS cluster and E(LS) is the electronic energy of the optimized LS cluster. As shown in Table 1, the spin energy of all of the clusters is less than zero, indicating that the HS state is lower in energy than the LS state. This result is in agreement with the experimental observation of only HS exchanged cobalt.[6,7] All other calculated results are reported for HS cobalt only.

Cobalt Exchange Stability. The relative stability of cobalt in each extraframework site was evaluated by computing the binding energy:

$$E_{bind} = E(\mathrm{Co{-}Z}) - E(\mathrm{Co}^{2+}) - E(\mathrm{Z}^{2-}) \quad (2)$$

where $E(Co^{2+})$ is the electronic energy of an isolated HS cobalt cation and $E(Z^{2-})$ is the electronic energy of the zeolite cluster optimized in the absence of cobalt. The unrealistic chemical reaction representing binding between cobalt and the zeolite leads to very large negative binding energies (Table 2). However, the relative values may be used, with some caution, to compare the stability of cobalt in the different sites. More negative binding energies correspond to stronger cobalt binding. The binding strength, from most strongly bound to least strongly bound, is B-1,4 > B-1,3 > B-2,5 > B-2,6 for the B site and G-1,4 > G-1,3 > G-2,6 > G-2,5 for the G site. The cobalt B site binding strength order agrees with the distance between aluminum atoms in the XRD structure. However, the order of the G site binding energies does not follow from the FER crystallographic coordinates.

Cluster Geometry. The structural features of the eight clusters are tabulated in Table 2. The structure and labeling convention of the cobalt clusters are shown in Figures 2−5. The distance between the cobalt and the immediate framework oxygen atoms is approximately 2 Å, in agreement with previous DFT calculations on cobalt-exchanged zeolites,[16,17,22] as well as the EXAFS results[13] reprinted in Table 3. As expected from ligand field theory, the HS cobalt−oxygen bond distances listed in Table 2 are slightly longer than the corresponding LS structures (not reported). In all of the clusters, the four oxygens that are nearest to cobalt are approximately planar. Cobalt in the B site sits above the oxygen plane, while cobalt in the G site sits in the plane of oxygens.

In all but one case, the structures of the B and G cobalt clusters with matching aluminum arrangements are very similar. The four shortest cobalt−oxygen bonds of the two 1,4 clusters

TABLE 1: Spin Energy (kJ/mol) and Cobalt Mulliken Population Analysis

	B-1,3	B-1,4	B-2,5	B-2,6	G-1,3	G-1,4	G-2,5	G-2,6
E_{spin}	−41.7	−41.1	−46.2	−45.5	−27.3	−20.9	−38.0	−50.5
				High Spin (HS)				
charge	0.74	0.63	0.84	0.82	0.80	0.78	0.84	0.85
spin density	2.61	2.61	2.61	2.59	2.61	2.61	2.65	2.64
				Low Spin (LS)				
charge	0.58	0.46	0.69	0.68	0.70	0.67	0.75	0.71
spin density	1.04	1.02	1.01	1.04	1.03	1.02	1.05	1.06

TABLE 2: Calculated Cobalt−FER Cluster Properties[a]

	B-1,3	B-1,4	B-2,5	B-2,6	G-1,3	G-1,4	G-2,5	G-2,6
E_{bind}	−2604	−2726	−2570	−2535	−2753	−2820	−2665	−2673
Co−O_a	2.01	2.02	1.94	1.97	1.99	1.98	1.96	2.05
Co−O_b	3.68	3.51	3.47	3.42	3.59	3.44	3.15	2.15
Co−O_c	1.96	2.02	2.16	2.13	1.94	1.98	2.21	2.22
Co−O_d	2.17	2.02	1.94	2.13	2.13	1.98	1.96	2.57
Co−O_e	3.31	3.51	3.47	3.41	3.24	3.44	3.15	3.68
Co−O_f	2.01	2.02	2.16	1.97	1.98	1.98	2.21	2.02
Co−T_1	2.69	2.74	2.80	2.77	2.84	2.80	2.96	2.87
Co−T_2	3.44	3.39	3.31	3.35	3.42	3.34	3.24	2.95
Co−T_3	3.35	3.39	3.45	3.41	3.26	3.34	3.35	3.02
Co−T_4	2.83	2.74	2.80	2.79	2.90	2.80	2.96	3.19
Co−T_5	3.40	3.39	3.31	3.41	3.30	3.34	3.24	3.78
Co−T_6	3.33	3.39	3.45	3.35	3.32	3.34	3.35	3.50
O_a−O_c	2.80	2.85	2.98	2.97	3.10	3.02	3.48	3.93
O_a−O_f	2.57	2.54	2.38	2.31	2.52	2.54	2.32	2.34
O_c−O_d	2.37	2.54	2.38	2.49	2.35	2.54	2.32	2.41
O_d−O_f	3.10	2.85	2.98	2.97	3.30	3.02	3.47	3.41

[a] All energies are reported in kJ/mol, and all distances are reported in Å. The T site labeling refers to relative position in the six-membered ring.

TABLE 3: EXAFS Interatomic Distances from Ref 13

	β signature		γ signature	
shell	distance (Å)	CN[a]	distance (Å)	CN[a]
Co−O	1.99	3.0	1.93	3.2
Co−O	2.09	1.7	2.00	1.3
Co−O	2.85	2.9	2.89	2.7
Co−Si/Al	3.32	2.3	3.30	2.8

[a] Coordination number.

are all equivalent for a given site, which is not surprising considering the approximate symmetry of the 1,4 clusters. The 1,3 clusters have three types of cobalt−oxygen bonds less than 3 Å. The Co−O_c bond is the shortest since the aluminum in position 3 is charge-compensated only through this oxygen. The longest bond, Co−O_d, is not directly involved in any charge compensation. The remaining bonds, Co−O_a and Co−O_f, are roughly equivalent, and the aluminum in position 1 is charge-compensated through both oxygens. The 2,5 clusters have two types of cobalt−oxygen bonds less than 3 Å. The approximate symmetry of this site leads to equivalent Co−O_a and Co−O_d bonds, which directly charge-compensates the aluminum centers, and longer Co−O_c and Co−O_f bonds that are not directly involved in charge compensation. The B-2,6 cluster has two types of short cobalt−oxygen bonds. The aluminum atoms are charge-compensated by cobalt through the short Co−O_a and Co−O_f bonds, while the noncharge-compensating Co−O_c and Co−O_d bonds are slightly longer. Unlike the other clusters, the G-2,6 cluster has five cobalt−oxygen bonds less than 3 Å. Although the starting geometry of this cluster possessed an approximate symmetry similar to the B-2,6 cluster, cobalt is more strongly associated with the aluminum in position 2 in the final structure. The Co−O_f bond is the shortest since the aluminum in position 6 is charge-compensated only through this oxygen. The other cobalt−oxygen bond lengths increase as Co−O_a < Co−O_b < Co−O_c. The longest cobalt−oxygen distance less than 3 Å, Co−O_d, does not charge-compensate either aluminum center and is too large to be considered a direct bond. In all cases but G-2,6, the Co−O_b and Co−O_e distances are longer than 3 Å, indicating no direct bonding with these framework oxygens.

The nearest silicon or aluminum centers to cobalt in all of the clusters except G-2,6 are the centers in the 1 and 4 positions. While the distances between cobalt and the 1 and 4 centers are equal for the 1,4, 2,5, and B-2,6 clusters, cobalt is slightly closer to the aluminum in position 1 than the silicon in position 4 for the 1,3 clusters. The remaining four silicon and aluminum centers in the ring are at least 3.2 Å away from cobalt. The two closest tetrahedral atoms to cobalt in the G-2,6 cluster are, in order, the silicon in position 1 and the aluminum in position 2.

IR Frequencies. Infrared spectroscopy investigations of cobalt-exchanged FER have proposed that cobalt perturbs zeolite framework stretching bands.[13,37] The calculated cobalt geometries confirm that cobalt distorts the FER framework as compared to the XRD structure of FER. The O_a−O_c and O_d−O_f interatomic distances (Table 2) are considerably shorter for the cobalt clusters as compared to the sodium FER XRD structure.[27] Cobalt induces a "contraction" in this direction by spanning the ring. Experiments have demonstrated that sodium-exchanged FER has an infrared transmission window from approximately 800 to 980 cm^{-1} that contains no features. Upon the exchange of cobalt, a new feature appears in this range.

IR frequencies were calculated for each cobalt cluster. Because the terminal groups of the clusters were held fixed, numerous imaginary frequencies were found. The fixed atoms also contribute additional real frequencies and couple with the vibrations of other atoms. The vibrations associated with the fixed atoms were eliminated by level-shifting the force constants associated with those atoms before determining the eigenvalues of the Hessian matrix.[38] The Hessian matrix elements corre-

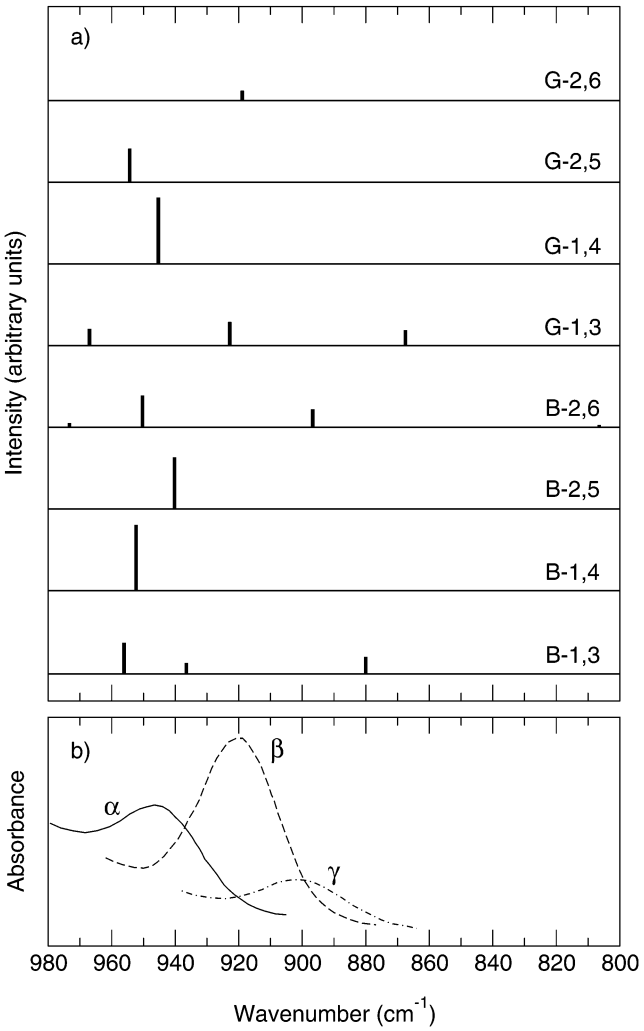

Figure 6. Infrared spectra of cobalt−FER in the transmission window 800−980 cm^{-1}; (a) calculated results for each cluster and (b) experimental signatures reproduced from ref 13.

sponding to the fixed atoms are negative; the level-shift procedure shifts all of these force constants to very large positive values. As a result, the vibrational modes corresponding to vibrations of the fixed atoms are shifted to very large wavenumbers, greater than 10 000 cm^{-1}, which are then discarded. This procedure eliminated all of the imaginary frequencies as well as the real frequencies associated with the fixed atoms. In addition, the transition dipole of each frequency, which is directly proportional to the intensity, was calculated using the atomic displacements and reduced masses produced by the level-shifting technique.[39]

The calculated frequencies and intensities of the IR bands for the cobalt clusters are shown in Figure 6a. All of the cobalt clusters have at least one mode between 800 and 980 cm^{-1}, and all of the vibrations in this window correspond to framework modes. The B-1,4, B-2,5, G-1,4, G-2,5, and G-2,6 cobalt clusters have a single vibration, while the B-1,3, B-2,6, and G-1,3 clusters have multiple vibrations.

Ultraviolet/Visible Spectra. Quantum chemical calculations of the ultraviolet/visible spectra of the cobalt clusters were carried out but were unsatisfactory. The intermediate neglect of differential overlap (INDO)/s[40] (ZINDO), configuration interaction singles[41] (CIS), and time-dependent DFT[42] (TD-DFT) methods could not produce the quantitative accuracy required to assign ultraviolet/visible signatures to particular cobalt environments. While these methods could qualitatively distinguish between tetrahedral cobalt, $CoCl_4^{2-}$, and octahedral cobalt, $Co(H_2O)_6^{2+}$, they could not quantitatively predict the optical spectra of these reference compounds. Higher level calculations that include spin−orbit coupling have successfully predicted the ultraviolet/visible spectra of cobalt-exchanged zeolites;[16] however, those calculations are beyond the scope of the present study.

Discussion

Wichterlová and co-workers assigned deconvoluted cobalt spectroscopic signatures to correspond to cobalt in particular extraframework sites;[9,13] cobalt in the B site was assigned to the α signature, while cobalt in the G site was assigned to the β signature. Cobalt was not directly observed in either of these sites; rather, the assignment was made based on similarities between the spectral signatures of mordenite and FER. While recent results indicate the importance of nearby aluminum centers,[43] experimental techniques have not been able to determine the arrangement of aluminum atoms in ion exchange sites. Meanwhile, computational studies with zeolite clusters containing different aluminum arrangements have only recently been reported,[19,23,24] and none have been reported for FER. The calculations carried out in this investigation are able to probe the role of aluminum arrangement and were used to evaluate the assignment of signatures to extraframework sites made by Wichterlová and co-workers. The calculated structure and infrared vibrations of the cobalt clusters were compared to the experimental EXAFS and infrared results to assign a signature to each of the clusters. Before evaluating each of the clusters to determine which signature they most closely match, some experimental and theoretical details are addressed.

Cobalt EXAFS data were collected for cobalt corresponding to the β and γ signatures by Sobalík et al.[13] EXAFS data cannot be easily deconvoluted into individual signatures, so only samples with one predominant type of cobalt were analyzed. The γ EXAFS was collected at very low cobalt loadings where γ cobalt predominates. At all other cobalt loadings, the majority of cobalt has the β signature allowing an EXAFS analysis of β cobalt. Cobalt with the α signature is always a minority species; hence, no EXAFS data exist for this signature. The EXAFS interatomic distances and coordination numbers are the results of a multivariable fitting procedure. The reported data are the result of 12 fitting parameters: the interatomic distance, coordination number, and Debye−Waller factor for four shells, or pairs of atoms. The quality of the fit depends in a complex manner on all of these parameters as well as the choice of shells.[44] However, the phase of the EXAFS function, χ, in *k*-space is primarily a function of interatomic distances, while the amplitude is a function of the shell choice, coordination number, and Debye−Waller factor. Hence, the interatomic distances are generally accurate, while the other parameters, including the choice of shell, are less reliable since they can more easily mask errors in each other. The experimental EXAFS distances and coordination numbers are given in Table 3. The experimental β and γ EXAFS results show two types of intimate cobalt−oxygen bonds and a longer cobalt−oxygen bond between 2.8 and 2.9 Å. The reported EXAFS cobalt−silicon/aluminum distance of 3.3 Å is considerably longer than any of the reported cobalt−oxygen distances.

The calculated infrared modes in Figure 6a can also be used to assign cobalt sites to signatures. Quantum chemical calculations are well-known to slightly overpredict the wavenumber of infrared modes. While no standard scaling factor has been reported for this particular combination of DFT functional and

basis set, DFT generally overpredicts infrared modes by approximately 1%.[45] No scaling factor was applied to the calculated values. The experimental α, *β*, and *γ* signatures correspond to deconvoluted IR peaks centered at 942, 918, and 905 cm^{-1}, respectively (Figure 6b).

B-1,3 and G-1,3. As previously noted, the calculated structures of the B and G clusters with matching aluminum arrangements are generally very similar. The three shortest cobalt−oxygen bonds of the B-1,3 and G-1,3 clusters compare very favorably with the *β* EXAFS distance (1.99 Å) and coordination number (3.0) (Tables 2 and 3). The two shortest *γ* EXAFS distances are also similar to the calculated distances. The calculated $Co-O_d$ bond lengths have a counterpart in the second cobalt−oxygen *β* EXAFS shell (2.09 Å) but not in the *γ* EXAFS; the G-1,3 cluster (2.13 Å) agrees more closely than the B-1,3 cluster (2.17 Å). The third EXAFS shell of both signatures (2.85 or 2.89 Å), if reinterpreted as a cobalt−silicon/aluminum distance, also has counterparts in the $Co-T_1$ and $Co-T_4$ distances of both clusters; again, the G-1,3 cluster more closely agrees than the B-1,3 cluster. To test the hypothesis that the EXAFS distance of 2.85 Å corresponds to a cobalt−silicon/aluminum distance, the EXAFS function for the G-1,3 cluster was calculated with the FEFF software package.[46] Without using any fitting parameters, the G-1,3 cluster qualitatively agreed very well with the experimental *χ* of the *β* signature (not shown). Finally, the fourth EXAFS shell (3.3 Å) matches several of the calculated cobalt−silicon/aluminum distances. The G-1,3 structure very closely matches the *β* EXAFS signature, while the B-1,3 cluster is similar but does deviate from the experimental signature.

As observed in Figure 6a, both clusters have three IR frequencies in the transmission window of interest. The lowest wavenumber mode in both spectra does not match any of the experimental signatures. The middle and more intense vibration of the G-1,3 cluster at 923 cm^{-1} slightly overpredicts the wavenumber of the center of the *β* signature, 918 cm^{-1}. The largest wavenumber G-1,3 vibration does not match any of the experimental signatures. Either of the larger wavenumber B-1,3 peaks at 937 or 956 cm^{-1} can be assigned to the α IR peak centered at 942 cm^{-1}. If the relative magnitude of the peaks is correct, then the vibration at 956 cm^{-1} can be conditionally assigned to match the α signature. The relative magnitude of calculated infrared intensities varies with basis set,[47] so the intensity of the two smaller vibrations may be overestimated as compared to the larger modes for this basis set. In contrast to the agreement between the calculated B-1,3 structure and the *β* EXAFS signature, the calculated infrared spectrum does not match the *β* signature. However, the calculated *β* signatures of the G-1,3 clusters are consistent with both IR and EXAFS and strongly suggest that cobalt in the G-1,3 site gives rise to the *β* signature.

B-1,4 and G-1,4. The geometries of the B-1,4 and G-1,4 clusters around the cobalt cation are nearly identical. Both clusters have four short cobalt−oxygen bonds that agree very well with the first *β* EXAFS shell (Tables 2 and 3). Like the 1,3 clusters, the third EXAFS shell of 2.85 Å closely matches calculated cobalt−aluminum distances rather than a cobalt−oxygen distance. However, neither cluster has a cobalt−oxygen distance that corresponds to the second *β* EXAFS shell of 2.09 Å. The two 1,4 clusters also have similar infrared signatures. The 952 and 945 cm^{-1} peaks are the only calculated vibrations for the B-1,4 and G-1,4 clusters, respectively. These calculated wavenumbers slightly overpredict the center of the experimental α IR peak at 942 cm^{-1}.

TABLE 4: Assignment of Cobalt−FER Signature to Cluster Model

signature	cluster
α	B-1,4; B-2,5; G-1,4; G-2,5
β	G-1,3
γ	none
none	B-1,3; B-2,6; G-2,6

B-2,5 and G-2,5. Once again, the structural similarity of the B- and G-2,5 clusters is a consequence of the matching symmetry of the aluminum substitutions. The B-2,5 and G-2,5 clusters have two short cobalt−oxygen bonds and two cobalt−silicon bonds that match the first and third *β* EXAFS shells, respectively (Tables 2 and 3). The clusters also have slightly longer cobalt−oxygen bonds that are similar to the second *β* EXAFS distance of 2.09 Å. The 2.16 Å B-2,5 distance agrees more closely than the 2.21 Å G-2,5 distance.

The infrared spectra of these two clusters clearly do not match the experimental *β* signature (Figure 6). The calculated 940 cm^{-1} B-2,5 and 954 cm^{-1} G-2,5 vibrations most closely agree with the experimental α IR signature (942 cm^{-1}). This vibrational mode of the 2,5 clusters is identical to the motion of the framework atoms in the 1,4 clusters. The 2,5 clusters are similar to the experimental *β* EXAFS signature and the α IR signature, like the B-1,3 cluster. However, in direct contrast to the ambiguity of the B-1,3 IR assignment, the 2,5 clusters clearly match the experimental α IR signature.

B-2,6 and G-2,6. Unlike the other three relative aluminum arrangements, the B-2,6 and G-2,6 clusters are structurally dissimilar. The calculated 2.57 Å G-2,6 cobalt−oxygen distance does not correspond to any EXAFS distance (Tables 2 and 3). The 1.97 and 2.13 Å B-2,6 cobalt−oxygen bonds agree with the first and second *β* EXAFS shells, respectively. Once again, the third EXAFS shell agrees with cobalt−silicon distances, $Co-T_1$ and $Co-T_4$. The calculated infrared vibrations of the 2,6 clusters are also different (Figure 6). The G-2,6 mode at 919 cm^{-1} is only one wavenumber larger than the center of the *β* peak at 918 cm^{-1}. The B-2,6 peak at 897 cm^{-1} is in close agreement with the experimental *γ* signature (905 cm^{-1}), while the peak at 950 cm^{-1} matches the experimental α signature. The 2,6 calculated results are irreconcilable; the G-2,6 structure clearly does not match the *β* EXAFS signature, while the infrared vibration is nearly a perfect match with the *β* signature, and the B-2,6 cluster cannot generate both the α and the *γ* infrared signatures as the calculations would suggest.

Assignment of Signatures. Because only one cluster, G-1,3, matched both the *β* EXAFS and the IR signatures, it can be unambiguously assigned to the *β* signature (Table 4). Unexpectedly, multiple clusters matched the α signature, B-1,4, B-2,5, G-1,4, and G-2,5. Only the calculated B-1,4 and B-2,5 signatures were anticipated by experiment. The relative values of the cobalt binding energy suggest that the G-2,5 cluster is not as likely a cobalt extraframework site as G-1,4, nor is the B-2,5 as likely as the B-1,4, assuming that the empty sites are equally probable. Without a second signature, like EXAFS, to further distinguish between these four clusters, definitive assignment of the α signature is not possible. However, even with an α EXAFS signature, the structures of the B-1,4 and G-1,4 clusters are too similar to be distinguished. The cobalt bond distances of the B-2,5 and G-2,5 clusters are also very similar to each other and the *β* EXAFS signature. An ultraviolet/visible spectra calculation may be able to further distinguish the four α candidate clusters.

In principle, all of the clusters considered are potential cobalt extraframework sites. However, the calculated properties of the remaining clusters strongly suggest that they are either not

present in FER or, if present, are not occupied by cobalt. Three of the cluster models, B-1,3, B-2,6, and G-2,6, either do not match any or match contradictory experimental signatures. The irreconcilable properties of the G-2,6 cluster, matching the β IR signature but not the β EXAFS signature, exclude it as a possible cobalt extraframework site. The B-2,6 cluster matches both the α and the γ IR signatures but the β EXAFS signature, another seemingly contradictory result. The B-1,3 weakly matches the β EXAFS signature and the α IR signature; this cluster is excluded because of the weak agreement with any signature rather than the contradiction between the two. On the basis of these results, these clusters are not considered potential extraframework sites for cobalt.

Even without additional experimental or theoretical data, one of the candidate α clusters is considered most likely based on other, more indirect experimental evidence. During calcination, the intensity of the α signature decreases and is accompanied by a corresponding increase in the β signature.[13] This observation has been interpreted as the migration of cobalt ions from sites with the α signature to sites with the β signature. On the basis of the relative values of the binding energies, cobalt is most strongly bound in the α signature G-1,4 site. One would not expect cobalt to migrate from this site to the less strongly bound G-1,3 site with the β signature, suggesting that the G-1,4 site is not occupied. The B-1,4, B-2,5, and G-2,5 binding energies are less favorable than the G-1,3 binding energy and would lead to the correct experimental observation. The binding energy of cobalt in the B-1,4 site is more favorable than in the B-2,5 or G-2,5 sites, suggesting that the B-1,4 site would be the first α site to be occupied by cobalt.

Additionally, the majority of the G sites must have 1,3 aluminum arrangements. At the highest possible cobalt loading (Co/Al = 0.5), each FER (Si/Al $\approx$ 8−9) unit cell contains, on average, slightly less than two cobalt ions. The FER unit cell contains a total of two G extraframework sites. The predominant observed signature is β; therefore, the predominant aluminum arrangement of the G site must be G-1,3. Consequently, few G sites are available for alternative aluminum arrangements such as G-1,4 or G-2,5. The B-1,4 and B-2,5 sites do not suffer from this numerical restriction. The B-1,4 cluster is the only cluster than generates an α IR signature that is consistent with all of the available evidence and hence is considered the most likely candidate to correspond to the α signature. However, the evidence for this cluster over the B-2,5, G-1,4, and G-2,5 clusters is indirect, and a combination of more than one of these clusters is possible.

Conclusions

The computed cobalt signatures were found to depend on the relative arrangement of aluminum atoms in the extraframework site. The cobalt B-1,4, B-2,5, G-1,4, and G-2,5 clusters were all determined to have the α signature, while only the G-1,3 cluster calculation produced the β signature. The B-2,6 and G-2,6 clusters were predicted to have inconsistent IR and EXAFS signatures, while the B-1,3 did not match any of the signatures well. Other, more indirect evidence suggests that the α signature is mainly due to cobalt in the B-1,4 site.

This conclusion agrees with the original site/signature assignment proposed by Wichterlová and co-workers that the α signature is due to cobalt in the B site while the β signature arises from cobalt in the G site. However, these results also demonstrate that the correlation of G-1,4 geometrical and electrostatic properties to the β infrared signature by Šponer et al.[22] is ultimately incorrect. The β signature is solely due to the G-1,3 cluster, while the G-1,4 cluster actually corresponds to the α signature. These calculations also add additional information regarding the likely arrangement of aluminum atoms in these sites. For the 1,4 and 2,5 clusters, similar structures and infrared spectra were found for both extraframework sites. The observed signature is not an intrinsic property of an extraframework site, but rather a given signature could, in principle, correspond to cobalt in multiple extraframework sites. With the knowledge of both the extraframework site and the relative aluminum arrangement in that site, future calculations can be performed to evaluate the catalytic activity of cobalt as a function of its local zeolite environment.

Acknowledgment. We thank Wolfgang Sachtler for insightful discussions, Jean-François Gaillard and Sam Webb for their assistance with the FEFF calculations, and an anonymous reviewer for helpful comments. This work was supported by the EMSI program of the National Science Foundation and the Department of Energy (CHE-9810378) at the Northwestern University Institute for Environmental Catalysis. Additional support was provided by the National Computational Science Alliance (CTS010016N) utilizing the NCSA Origin 2000.

References and Notes

(1) Traa, Y.; Burger, B.; Weitkamp, J. *Microporous Mesoporous Mater.* **1999**, *30*, 3−41.
(2) Li, Y.; Armor, J. N. *Appl. Catal., B* **1992**, *1*, L31−L40.
(3) Armor, J. N. *Catal. Today* **1995**, *26*, 147−158.
(4) Wang, X.; Chen, H.-Y.; Sachtler, W. M. H. *Appl. Catal., B* **2000**, *26*, L227−L239.
(5) Wang, X.; Chen, H.; Sachtler, W. M. H. *Appl. Catal., B* **2001**, *29*, 47−60.
(6) Li, Y.; Slager, T. L.; Armor, J. N. *J. Catal.* **1994**, *150*, 388−399.
(7) El-Malki, E.-M.; Werst, D.; Doan, P. E.; Sachtler, W. M. H. *J. Phys. Chem. B* **2000**, *104*, 5924−5931.
(8) Li, Y.; Armor, J. N. *J. Catal.* **1994**, *150*, 376−387.
(9) Kaucký, D.; Dédeček, J.; Wichterlová, B. *Microporous Mesoporous Mater.* **1999**, *31*, 75−87.
(10) Kaucký, D.; Vondrová, A.; Dédeček, J.; Wichterlová, B. *J. Catal.* **2000**, *194*, 318−329.
(11) Dédeček, J.; Wichterlová, B. *J. Phys. Chem. B* **1999**, *103*, 1462−1476.
(12) Dédeček, J.; Kaucký, D.; Wichertlová, B. *Microporous Mesoporous Mater.* **2000**, *35*−*36*, 483−494.
(13) Sobalík, Z.; Dédeček, J.; Wichterlová, B.; Drozdová, L.; Prins, R. *J. Catal.* **2000**, *194*, 330−342.
(14) Mortier, W. J. *Compilation of Extraframework Sites in Zeolites*; Butterworth Scientific: London, 1982.
(15) Schneider, W. F.; Hass, K. C.; Ramprasad, R.; Adams, J. B. *J. Phys. Chem. B* **1997**, *101*, 4353−4357.
(16) Pierloot, K.; Delabie, A.; Ribbing, C.; Verberckmoes, A. A.; Schoonheydt, R. A. *J. Phys. Chem. B* **1998**, *102*, 10789−10798.
(17) Rice, M. J.; Chakraborty, A. K.; Bell, A. T. *J. Phys. Chem. A* **1998**, *102*, 7498−7504.
(18) Rice, M. J.; Chakraborty, A. K.; Bell, A. T. *J. Phys. Chem. B* **2000**, *104*, 9987−9992.
(19) Nachtigallová, D.; Nachtigall, P.; Sauer, J. *Phys. Chem. Chem. Phys.* **2001**, *3*, 1552−1559.
(20) Nachtigall, P.; Davidová, M.; Nachtigallová, D. *J. Phys. Chem. B* **2001**, *105*, 3510−3517.
(21) Shubin, A. A.; Zhidomirov, G. M.; Yakovlev, A. L.; van Santen, R. A. *J. Phys. Chem. B* **2001**, *105*, 4928−4935.
(22) Šponer, J. E.; Sobalík, Z.; Leszczynski, J.; Wichterlová, B. *J. Phys. Chem. B* **2001**, *105*, 8285−8290.
(23) Pierloot, K.; Delabie, A.; Groothaert, M. H.; Schoonheydt, R. A. *Phys. Chem. Chem. Phys.* **2001**, *3*, 2174−2183.
(24) Delabie, A.; Pierloot, K.; Groothaert, M. H.; Weckhuysen, B. M.; Schoonheydt, R. A. *Phys. Chem. Chem. Phys.* **2002**, *4*, 134−145.
(25) Broadbelt, L. J.; Snurr, R. Q. *Appl. Catal., A* **2000**, *200*, 23−46.
(26) Löwenstein, W. *Am. Mineral.* **1954**, *39*, 92−96.
(27) Vaughan, P. A. *Acta Crystallogr.* **1966**, *21*, 983−990.
(28) Feng, X.; Hall, W. K. *Catal. Lett.* **1997**, *46*, 11−16.
(29) Rice, M. J.; Chakraborty, A. K.; Bell, A. T. *J. Catal.* **1999**, *186*, 222−227.
(30) Rice, M. J.; Chakraborty, A. K.; Bell, A. T. *J. Catal.* **2000**, *194*, 278−285.

(31) Becke, A. D. *Phys. Rev. A* **1988**, *38*, 3098−3100.
(32) Perdew, J. P. *Phys. Rev. B* **1986**, *33*, 8822−8824.
(33) Frisch, M. J.; Trucks, G. W.; Schlegel, H. B.; Scuseria, G. E.; Robb, M. A.; Cheeseman, J. R.; Zakrzewski, V. G.; Montgomery, J. A., Jr.; Stratmann, R. E.; Burant, J. C.; Dapprich, S.; Millam, J. M.; Daniels, A. D.; Kudin, K. N.; Strain, M. C.; Farkas, O.; Tomasi, J.; Barone, V.; Cossi, M.; Cammi, R.; Mennucci, B.; Pomelli, C.; Adamo, C.; Clifford, S.; Ochterski, J.; Petersson, G. A.; Ayala, P. Y.; Cui, Q.; Morokuma, K.; Malick, D. K.; Rabuck, A. D.; Raghavachari, K.; Foresman, J. B.; Cioslowski, J.; Ortiz, J. V.; Baboul, A. G.; Stefanov, B. B.; Liu, G.; Liashenko, A.; Piskorz, P.; Komaromi, I.; Gomperts, R.; Martin, R. L.; Fox, D. J.; Keith, T.; Al-Laham, M. A.; Peng, C. Y.; Nanayakkara, A.; Gonzalez, C.; Challacombe, M.; Gill, P. M. W.; Johnson, B.; Chen, W.; Wong, M. W.; Andres, J. L.; Gonzalez, C.; Head-Gordon, M.; Replogle, E. S.; Pople, J. A. *Gaussian 98*, revision A.7; Gaussian, Inc.: Pittsburgh, PA, 1998.
(34) Jensen, F. *Introduction to Computational Chemistry*; John Wiley & Sons: Chincester, England, 1999.
(35) Bauernschmitt, R.; Ahlrichs, R. *J. Chem. Phys.* **1996**, *104*, 9047−9052.
(36) Mulliken, R. S. *J. Chem. Phys.* **1955**, *23* (10), 1833−1840.
(37) Sobalík, Z.; Tvarůžková, Z.; Wichterlová, B. *J. Phys. Chem. B* **1998**, *102*, 1077−1085.
(38) Jensen, F. Personal communication, 2001.
(39) Person, W. B., Zerbi, G., Eds. Vibrational Intensities in Infrared and Raman Spectroscopy. *Studies in Physical and Theoretical Chemistry*; Elsevier: New York, 1982; Vol. 20.
(40) Zerner, M. C.; Loew, G. H.; Kirchner, R. F.; Mueller-Westerhoff, U. T. *J. Am. Chem. Soc.* **1980**, *102*, 589−599.
(41) Foresman, J. B.; Head-Gordon, M.; Pople, J. A.; Frisch, M. J. *J. Phys. Chem.* **1992**, *96*, 135−149.
(42) Petersilka, M.; Gossmann, U. J.; Gross, E. K. U. *Phys. Rev. Lett.* **1996**, *76*, 1212−1215.
(43) Bortnovsky, O.; Sobalík, Z.; Wichterlová, B. *Microporous Mesoporous Mater.* **2001**, *46*, 265−275.
(44) Teo, B. K. EXAFS: Basic Principles and Data Analysis. *Inorganic Chemistry Concepts*; Springer-Verlag: Berlin, 1986; Vol. 9.
(45) Scott, A. P.; Radom, L. *J. Phys. Chem.* **1996**, *100*, 16502−16513.
(46) Ankudinov, A. L.; Ravel, B.; Rehr, J. J.; Conradson, S. D. *Phys. Rev.* **1998**, *B58*, 7565−7576.
(47) Chong, D. P.; Bree, A. V. *Chem. Phys. Lett.* **1993**, *210*, 443−447.